

# Unsteady MHD dusty fluid flow over a cone in the vicinity of porous medium: a numerical study

Hajar Hanafi <sup>a</sup>, Hanifa Hanif <sup>a,b</sup> and Sharidan Shafie <sup>a</sup>

<sup>a</sup>Department of Mathematical Sciences, Faculty of Science, Universiti Teknologi Malaysia, Johor Bahru, Johor, Malaysia; <sup>b</sup>Department of Mathematics, Sardar Bahadur Khan Women's University, Quetta, Pakistan

## ABSTRACT

This research presents an unsteady free convection magnetohydrodynamics (MHD) dusty fluid flow over a vertical cone enclosed inside a porous medium. The Crank–Nicolson approach is used to get the numerical solutions for these non-linear partial differential equations (PDEs). The velocity and temperature distributions are graphed numerically for a wide range of physical parameters to highlight important characteristics of the solutions. The results showed that increasing the porosity parameter leads to a rise in the velocity profile for the fluid and dust phases, while doing the reverse with the rise of the magnetic parameter, fluid-particle interaction parameter, and mass concentration of the particle phase parameter. Additionally, it is shown that the temperature profile rises as the magnetic parameter and the mass concentration of particle phase parameter grow, whereas the fluid-particle interaction parameter and porosity parameter show the opposite tendency.

## ARTICLE HISTORY

Received 29 November 2023  
Revised 2 April 2024  
Accepted 23 April 2024

## KEYWORDS



Dusty fluid;  
magnetohydrodynamic;  
Crank–Nicolson method;  
cone

## 1. Introduction

Dusty fluid may be found in a variety of engineering applications and natural events. Its significance is concentrated not only on the fundamental interest of fluid mechanics but also on economic, social, and environmental consequences owing to its applications in numerous forms of processes in the automotive, chemical, coating, and environmental industries. The experimental study published by Sproull [1] on the motion of the air flow carrying small dust particles has piqued the curiosity of many scientists to comprehend the phenomenon. Many investigations have been conducted by researchers, either experimentally or conceptually, regarding the problem of fluid-containing dust particle flow in order to elucidate the interaction between fluid and dust particles. Siddiqa et al. [2] explored the dusty fluid flow numerically by discussing important two-phase mechanisms. Their findings were created over a broad range of Prandtl number and as the mass concentration parameter and Prandtl number are high, extremely thin boundary layer structures may be generated. The rotating flow problem of fluid-particle interaction with the wall slip mechanism impacts has been investigated recently by Turkyilmazoglu [3]. They observed that the fluid-particle interaction parameter decreases the fluid temperature while increasing the particle temperature. Consequently, greater interaction leads to surface cooling of the fluid. Dey et al. [4] discussed the viscous dusty fluid behaviour flowing over

an elongating curved plate in the presence of a dust volume fraction. They found that an augmentation in the volume fraction parameter results in the thermal boundary layer width enhancement for both phases. There are several interesting studies on the heat transfer rates of dusty fluids in various geometries that can be found in [5–8].

Initiated by Platzman [9], the process of evaluating the behaviour of electrically conducting fluids and magnetic characteristics is known as MHD. The magnetic field and velocity field are essentially interacting in this case. In other words, both motion and the magnetic field have an impact on each other. MHD flow is a crucial field for research because of its potential uses [10]. The studies on the effects of MHD and nanoparticles in a fluids were conducted by Hanif and Shafie [11, 12]. These research demonstrated that the magnetic parameters frequently forecast the flow of Maxwell fluid augmentation and that the magnetic number parameters must be significant in order to enhance surface heat. It was reported that the magnetic parameter amplified as the velocity profile depreciated. Saqib et al. [13] used the fractional Cattaneo-Friedrich Model to explore heat transmission in magnetic Maxwell fluid flow. The outcomes suggested that the fractional parameters have a considerable influence on the temperature and velocity distribution. It was discovered that when the fractional parameter was increased, the temperature field rose. The influence of fractional parameters, on the

**CONTACT** Hanifa Hanif  hanifahanif@outlook.com  Department of Mathematical Sciences, Faculty of Science, Universiti Teknologi Malaysia, Johor Bahru, Johor, 81310, Malaysia, Department of Mathematics, Sardar Bahadur Khan Women's University, Quetta, Pakistan

© 2024 The Author(s). Published by Informa UK Limited, trading as Taylor & Francis Group.

This is an Open Access article distributed under the terms of the Creative Commons Attribution-NonCommercial License (<http://creativecommons.org/licenses/by-nc/4.0/>), which permits unrestricted non-commercial use, distribution, and reproduction in any medium, provided the original work is properly cited. The terms on which this article has been published allow the posting of the Accepted Manuscript in a repository by the author(s) or with their consent.

other hand, is inversely related to the velocity field near the plate. Recent research by Abbas et al. [14] has investigated how MHD dusty fluid movement transmits heat and mass. It was discovered that the temperature distribution was improved using the thermal radiation parameter. Moreover, the velocities of the fluid and dust are more evenly distributed when the Hall parameter is increased, and boosting the slip parameter causes the velocities to rise. The fluctuation in the Hall and ion slip parameters has an inverse relationship with the fluid and particle temperatures. Hanif et al. [15, 16] investigated MHD CdTe nanofluid flow inside porous medium. The findings showed that the system's thermal performance improves due to thermal radiation and magnetic fields. In the meantime, a change in viscosity lowers the temperature while increasing the velocity profile. As the velocity distribution drops, resistive forces are produced, hence, the magnetic field rises. As the permeability coefficient was maximized while being enhanced for higher temperatures of thermal radiation, the momentum decreased. A few enticing and motivating facts about MHD are given in [17–20].

Fluid motion across a cone geometry has sparked tremendous attention due to the multiple heat transfer applications. Despite its relevance in the disciplines of technology and engineering, examining the flow characteristics of fluids is extremely challenging. It may be found in a variety of industrial uses as well as in natural settings. Researchers face difficulties in formulating the problem because of the angle parameter of the cone when it is positioned vertically. Owing to this fact, numerous authors have written on convective flow over a vertical cone since 1953. A groundbreaking study by Merk and Prins [21] looked at flow over a cone and found universal relationships for equivalent solutions to a process that happens at constant temperature in axisymmetric shapes. Awad et al. [22] investigated numerically a cone situated within a porous medium featuring cross-diffusion. They found that increasing permeability corresponds to a decline in the heat transfer rate. Makanda et al. [23] examined convective behaviour occurring in a viscoelastic fluid within porous media, emanating from a cone oriented in a downward direction. An escalation in the porosity parameter was noted to coincide with a decrease in the velocity profile, accompanied by reductions in both Nusselt number and shear stress. Conversely, the temperature profile exhibited the opposite effect. Jasmine Benazir et al. [24] examined the influence of dispersion effects over a vertical cone and a flat plate saturated with porous media. They observed a decrease in fluid flow with an augmentation in the parameter of magnetic field, while the porous permeability parameter exhibited the opposite trend. Additionally, temperature profiles tended to decrease with higher Prandtl number levels. Hanif et al. [25] discussed Maxwell fluid flow over a cone embedded in a porous media with non-Newtonian

heating. Basha et al. [26] analyzed the chemically reactive nanofluid flow across two geometries, a cone and plate when activation energy and a chemical reaction are present. Large values of the Hartmann number were found to reduce fluid velocity due to the resistive force, slowing down fluid motion and consequently enhancing heat transfer within the thermal boundary layer. Turkyilmazoglu [27] examined the disk-cone conical gaps filled with non-compressible viscous fluid and involves in convective heat transport. Ilyas et al. [28] examined the convective heat transfer periodic pattern along a MHD cone buried in a porous medium. In this case, steady-state solutions are used in the unsteady state to compute the periodic behaviour of physical quantities. The magnetic profile values improved with increasing magnetic parameters. On the contrary, the porous permeability parameter made it deteriorate.

On the subject of dusty flows in cones, research was done by Siddiq et al. [29, 30] on the characteristics of two-phase flows along a vertical cone. Results for both studies are analyzed by using metal as a solid phase and oil as the base fluid while taking into account several significant parameters. The key findings of this research are that the amount of metal particles in the oil has a substantial impact on the rate of heat transfer coefficient. Additionally, it has been discovered that particle loading increases drag forces for fluids like oil. Mahanthesh et al. [31] published an investigation of the flow of Casson dusty fluid over three distinct geometries. They observed that the presence of a magnetic field enhances the heat transfer rate. Additionally, suspended dust particles contribute to an increased heat transfer rate. Palani and Kumar [32] studied the movement of gas-containing dust particles over a semi-infinite vertical cone. They discovered that the particles of dust in the liquid reduce the velocity of dusty gas in contrast to the velocity of gas without dust, since the dusty particles hinder the flow of gas. Despite the fact that there has been a little research on the fluid containing dust particles flow over a vertical cone, they all mostly dealt with steady cases, see: [33, 34].

Fluid flow techniques such as Lagrangian and Eulerian can be used to explain the mathematical modelling of two-phase fluid and particle systems. While the latter perspective regards both phases as interacting continua coexisting in the same space, the former considers the liquid phase as a continuum with a dust cloud governed by kinetic theory [35]. As such, the particle phase will be included in this study using a dusty gas model, the interacting continua method that was suggested by Saffman [36]. The bulk of these fluid-related matters are linear and were formulated to address steady fluid phenomena. The present study investigates the magnetic fields influence on unsteady free convection of dusty fluid flow across a vertical cone embedded in a porous medium. The Crank–Nicolson method [37–39], along with the Thomas algorithm [40], is employed to

numerically solve the nonlinear, dimensionless, coupled partial differential equations. Numerical results are obtained using a custom algorithm implemented in MATLAB, which is extensively illustrated for clarity.

## 2. Mathematical formulation

This study focuses on the free convective flow of a dusty fluid over a vertical cone, delineated by a radius  $r$  (where  $r = x \sin \alpha$ ), while also incorporating the magnetic field influence. The cone's surface is aligned with the  $x$ -axis, while its normal direction is along the  $y$ -axis. It is presumed that the solid particles have a spherical form, with non-reactive properties and a constant size. Additionally, it is assumed that the particles' number density remains constant. Interactions between the particles, chemical reactions, and radiation between the particles and the liquid are not considered. The concentration of dust is considered to be so low that it does not significantly disrupt the continuity or the effects of MHD. Furthermore, the magnetic Reynolds number is presumed extremely low, rendering induced magnetic fields negligible. Consequently, only a consistent magnetic field aligned with the  $y$ -axis, as depicted in Figure 1, is expected to be the sole magnetic field considered in the problem. All external forces except for the gravitational force are disregarded.

The fundamental governing equations using the aforementioned assumption and boundary layer approximations are [2, 36, 41]:

### 2.1. Fluid phase

$$\nabla \cdot (r\mathbf{V}) = 0, \quad (1)$$

$$\rho \left( \frac{\partial u}{\partial t} + (\mathbf{V} \cdot \nabla) u \right) = \mu \frac{\partial^2 u}{\partial y^2} + g(\rho\beta_T) \cos \alpha (T - T_\infty) - \sigma B^2 u - \frac{\mu}{k_0} u + \frac{\rho_p}{\tau_m} (u_p - u), \quad (2)$$

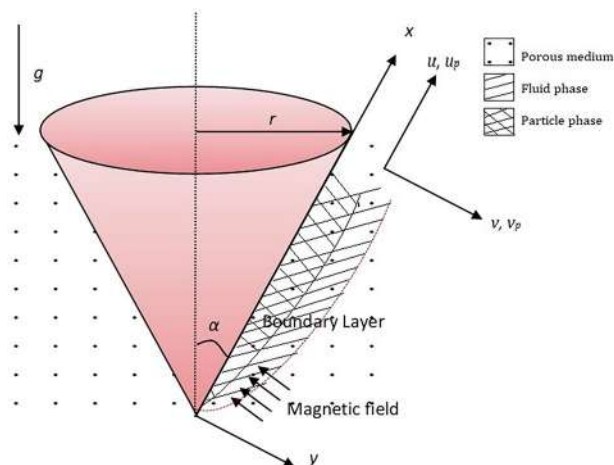


**Figure 1.** Geometric coordinates system and problem layouts.

$$\rho C_p \left( \frac{\partial T}{\partial t} + (\mathbf{V} \cdot \nabla) T \right) = k \frac{\partial^2 T}{\partial y^2} + \frac{\rho_p C_s}{\tau_T} (T_p - T), \quad (3)$$

### 2.2. Particle phase

$$\nabla \cdot (r\mathbf{V}_p) = 0, \quad (4)$$

$$\rho_p \left( \frac{\partial u_p}{\partial t} + (\mathbf{V}_p \cdot \nabla) u_p \right) = -\frac{\rho_p}{\tau_m} (u_p - u), \quad (5)$$

$$\rho_p C_s \left( \frac{\partial T_p}{\partial t} + (\mathbf{V}_p \cdot \nabla) T_p \right) = -\frac{\rho_p C_s}{\tau_T} (T_p - T), \quad (6)$$

where  $\nabla = (\frac{\partial}{\partial x}, \frac{\partial}{\partial y})$  is the gradient operator,  $(\mathbf{V}, \mathbf{V}_p) = ((u, v), (u_p, v_p))$  is the velocity components,  $(T, T_p) =$  temperature,  $(\rho, \rho_p) =$  density,  $g =$  gravitational force,  $\beta_T =$  volumetric thermal expansion coefficient with temperature,  $\tau_m =$  momentum relaxation time,  $\tau_T =$  thermal relaxation time,  $\alpha =$  cone half angle,  $B =$  magnetic field,  $\mu =$  dynamic viscosity,  $\sigma =$  electrical conductivity,  $k_0 =$  permeability constant,  $k =$  thermal conductivity,  $C_p =$  specific heat,  $k_e =$  absorption coefficient,  $\sigma_s =$  Stefan-Boltzmann. The initial and boundary conditions are,

$$\begin{aligned} u(x, y, 0) = 0, u_p(x, y, 0) = 0, v(x, y, 0) = 0, \\ v_p(x, y, 0) = 0, T(x, y, 0) = T_\infty, T_p(x, y, 0) = T_\infty, \\ u(x, 0, t) = 0, u_p(x, 0, t) = 0, v(x, 0, t) = 0, \\ v_p(x, 0, t) = 0, T(x, 0, t) = T_w, T_p(x, 0, t) = T_w, \\ u(0, y, t) = 0, u_p(0, y, t) = 0, T(0, y, t) = T_\infty, \\ T_p(0, y, t) = T_\infty, \\ u(x, y, t) \rightarrow 0, u_p(x, y, t) \rightarrow 0, T(x, y, t) \rightarrow T_\infty, \\ T_p(x, y, t) \rightarrow T_\infty, \text{ as } y \rightarrow \infty. \end{aligned} \quad (7)$$

Below are the corresponding physical measurements for the local shear stress and local Nusselt number,

$$\tau_x = \mu \left( \frac{\partial u}{\partial y} \right)_{y=0}, \quad (8)$$

$$Nu_x = \frac{-x \left( \frac{\partial T}{\partial y} \right)_{y=0}}{T_w - T_\infty}. \quad (9)$$

Using dimensionless parameter [42],

$$\begin{aligned} x^* = \frac{x}{L}, y^* = \frac{y}{L} (Gr_L)^{\frac{1}{4}}, R^* = \frac{r}{L}, \\ (v, v_p)^* = \frac{L}{v_f} (Gr_L)^{-\frac{1}{4}} (v, v_p), \\ (u, u_p)^* = \frac{L}{v_f} (Gr_L)^{-\frac{1}{2}} (u, u_p), t^* = \frac{v_f t}{L^2} (Gr_L)^{\frac{1}{2}}, \\ (T, T_p)^* = \frac{(T, T_p) - T_\infty}{T_w - T_\infty}. \end{aligned} \quad (10)$$

Equations (1)–(6) are subsequently transformed into the following dimensionless form, (for convenience,

remove \* sign)

$$\frac{\partial u}{\partial x} + \frac{\partial v}{\partial y} + \frac{u}{x} = 0, \quad (11)$$

$$\frac{\partial u}{\partial t} + u \frac{\partial u}{\partial x} + v \frac{\partial u}{\partial y} = \frac{\partial^2 u}{\partial y^2} + T \cos \alpha - \left(M + \frac{1}{K}\right) u + D_p \alpha_d (u_p - u), \quad (12)$$

$$\frac{\partial T}{\partial t} + u \frac{\partial T}{\partial x} + v \frac{\partial T}{\partial y} = \frac{1}{Pr} \frac{\partial^2 T}{\partial y^2} + \frac{2}{3Pr} D_p \alpha_d (T_p - T), \quad (13)$$

$$\frac{\partial u_p}{\partial x} + \frac{\partial v_p}{\partial y} + \frac{u_p}{x} = 0, \quad (14)$$

$$\frac{\partial u_p}{\partial t} + u_p \frac{\partial u_p}{\partial x} + v_p \frac{\partial u_p}{\partial y} = -\alpha_d (u_p - u), \quad (15)$$

$$\frac{\partial T_p}{\partial t} + u_p \frac{\partial T_p}{\partial x} + v_p \frac{\partial T_p}{\partial y} = -\frac{2}{3\gamma Pr} \alpha_d (T_p - T), \quad (16)$$

$Pr = \frac{\nu_f}{\alpha}$  is Prandtl number,  $D_p = \frac{\rho_p}{\rho}$  is mass concentration of particle phase parameter,  $\gamma = \frac{C_s}{C_p}$  is the specific heat ratio of mixture,  $\tau_T = \frac{3}{2} \gamma \tau_m Pr$  is the relation between  $\tau_T$  and  $\tau_m$ , indicating that  $\tau_T$  is obeying the Stokes law.  $\alpha_d = \frac{L^2}{\nu_f \tau_m} (Gr_L)^{-\frac{1}{2}}$  is the fluid-particle interaction parameter,  $M = \frac{\sigma B^2 L^2}{\mu} (Gr_L)^{-\frac{1}{2}}$  is magnetic field parameter and  $\frac{1}{K} = \frac{L^2}{k_0} (Gr_L)^{-\frac{1}{2}}$  is porous permeability parameter. The dimensionless initial and boundary conditions are as follows,

$$\begin{aligned} t \leq 0 : (u, u_p) &= 0, (v, v_p) = 0, (T, T_p) = 0 \text{ for all } x \text{ and } y, \\ t > 0 : (u, u_p) &= 0, (v, v_p) = 0, (T, T_p) = 1 \text{ at } y = 0, \\ (u, u_p) &= 0, (T, T_p) = 0 \text{ at } x = 0, \\ (u, u_p) &\rightarrow 0, (T, T_p) \rightarrow 0 \text{ as } y \rightarrow \infty. \end{aligned} \quad (17)$$

The dimensionless local shear stress and local Nusselt number are given by,

$$\tau_x = Gr_L^{\frac{3}{4}} \left( \frac{\partial u}{\partial y} \right)_{y=0}, \quad (18)$$

$$Nu_x = -Gr_L^{\frac{1}{4}} x \left( \frac{\partial T}{\partial y} \right)_{y=0}. \quad (19)$$

### 2.3. Numerical procedure of Crank–Nicolson

To mitigate programming challenges, it is necessary to convert the equations from a continuous to a discrete form. Through discretization of the dimensionless equations and conducting iterations denoted by  $i$  and  $j$ , the system is converted into a tridiagonal form. The following are finite difference equation analogous to Equations (11)–(16),

$$\begin{aligned} &\frac{u_{ij}^{k+1} - u_{i-1j}^{k+1} + u_{ij}^k - u_{i-1j}^k}{2\Delta x} \\ &+ \frac{v_{ij}^{k+1} - v_{ij-1}^{k+1} + v_{ij}^k - v_{ij-1}^k}{2\Delta y} \end{aligned}$$

$$+ \frac{1}{x_i} \frac{u_{ij}^{k+1} + u_{ij}^k}{2} = 0, \quad (20)$$

$$\begin{aligned} &\left( \frac{u_{ij}^{k+1} - u_{ij}^k}{\Delta t} \right) + u_{ij}^k \left( \frac{u_{ij}^{k+1} - u_{i-1j}^{k+1} + u_{ij}^k - u_{i-1j}^k}{2\Delta x} \right) \\ &+ v_{ij}^k \left( \frac{u_{ij+1}^{k+1} - u_{ij-1}^{k+1} + u_{ij+1}^k - u_{ij-1}^k}{4\Delta y} \right) \\ &= \frac{u_{ij+1}^{k+1} - 2u_{ij}^{k+1} + u_{ij-1}^{k+1} + u_{ij+1}^k - 2u_{ij}^k + u_{ij-1}^k}{2(\Delta y)^2} \\ &+ \frac{T_{ij}^{k+1} + T_{ij}^k}{2} \cos \alpha - \left(M + \frac{1}{K}\right) \frac{u_{ij}^{k+1} + u_{ij}^k}{2} \\ &+ D_p \alpha_d \left( \frac{u_{p_{ij}}^{k+1} + u_{p_{ij}}^k}{2} - \frac{u_{ij}^{k+1} + u_{ij}^k}{2} \right), \end{aligned} \quad (21)$$

$$\begin{aligned} &\left( \frac{T_{ij}^{k+1} - T_{ij}^k}{\Delta t} \right) + u_{ij}^k \left( \frac{T_{ij}^{k+1} - T_{i-1j}^{k+1} + T_{ij}^k - T_{i-1j}^k}{2\Delta x} \right) \\ &+ v_{ij}^k \left( \frac{T_{ij+1}^{k+1} - T_{ij-1}^{k+1} + T_{ij+1}^k - T_{ij-1}^k}{4\Delta y} \right) \\ &= \frac{1}{Pr} \left( \frac{T_{ij+1}^{k+1} - 2T_{ij}^{k+1} + T_{ij-1}^{k+1} + T_{ij+1}^k - 2T_{ij}^k + T_{ij-1}^k}{2(\Delta y)^2} \right) \\ &+ \frac{2}{3Pr} D_p \alpha_d \left( \frac{T_{p_{ij}}^{k+1} + T_{p_{ij}}^k}{2} - \frac{T_{ij}^{k+1} + T_{ij}^k}{2} \right), \end{aligned} \quad (22)$$

$$\begin{aligned} &\frac{u_{p_{ij}}^{k+1} - u_{p_{i-1j}}^{k+1} + u_{p_{ij}}^k - u_{p_{i-1j}}^k}{2\Delta x} \\ &+ \frac{v_{p_{ij}}^{k+1} - v_{p_{ij-1}}^{k+1} + v_{p_{ij}}^k - v_{p_{ij-1}}^k}{2\Delta y} \\ &+ \frac{1}{x_i} \frac{u_{p_{ij}}^{k+1} + u_{p_{ij}}^k}{2} = 0, \end{aligned} \quad (23)$$

$$\begin{aligned} &\left( \frac{u_{p_{ij}}^{k+1} - u_{p_{ij}}^k}{\Delta t} \right) \\ &+ u_{p_{ij}}^k \left( \frac{u_{p_{ij}}^{k+1} - u_{p_{i-1j}}^{k+1} + u_{p_{ij}}^k - u_{p_{i-1j}}^k}{2\Delta x} \right) \\ &+ v_{p_{ij}}^k \left( \frac{u_{p_{ij+1}}^{k+1} - u_{p_{ij-1}}^{k+1} + u_{p_{ij+1}}^k - u_{p_{ij-1}}^k}{4\Delta y} \right) \\ &= -\alpha_d \left( \frac{u_{p_{ij}}^{k+1} + u_{p_{ij}}^k}{2} - \frac{u_{ij}^{k+1} + u_{ij}^k}{2} \right), \end{aligned} \quad (24)$$

$$\begin{aligned} &\left( \frac{T_{p_{ij}}^{k+1} - T_{p_{ij}}^k}{\Delta t} \right) \\ &+ u_{p_{ij}}^k \left( \frac{T_{p_{ij}}^{k+1} - T_{p_{i-1j}}^{k+1} + T_{p_{ij}}^k - T_{p_{i-1j}}^k}{2\Delta x} \right) \end{aligned}$$

$$\begin{aligned}
 &+ v_{p_{ij}}^k \left( \frac{T_{p_{ij+1}}^{k+1} - T_{p_{ij-1}}^{k+1} + T_{p_{ij+1}}^k - T_{p_{ij-1}}^k}{4\Delta y} \right) \\
 &= -\frac{2}{3\gamma Pr} \alpha_d \left( \frac{T_{p_{ij}}^{k+1} + T_{p_{ij}}^k}{2} - \frac{T_{ij}^{k+1} + T_{ij}^k}{2} \right). \quad (25)
 \end{aligned}$$

### 3. Results

The Crank–Nicholson technique is used to solve an unstable, dimensionless PDE. The Thomas algorithm approach was then used to solve the equation system in time  $t$ . At  $y_{\max} = 20$  and  $x_{\max} = 1$ , the rectangular domain is taken into account. Given that  $y_{\max}$  and  $y_{\infty}$  are constant,  $y$  is assumed to be 20 in order to satisfy the boundary requirements in Equation (17).  $\Delta y = 0.05$ ,  $\Delta x = 0.05$ , and  $\Delta t = 0.01$  have been established to be the meshing sizes. When  $\Delta y$ ,  $\Delta x$ , and  $\Delta t$  approach the value of null, the shortness of ignorance is  $O(\Delta y^2 + \Delta t^2 + \Delta x)$ . From the previous calculations, predictions, and calculations, it is possible to draw the conclusion that an organized and complicated plan of action shows that a solution may appear and work in harmony, as shown in Refs. [43–45]. The modifying parameters outcomes on the distributions of velocity and temperature are explored. The numerical assessment results for  $M$ ,  $Rd$ ,  $Q$ ,  $K$ ,  $Pr$ ,  $\alpha_d$ ,  $D_p$ , and  $\gamma$  are visually depicted. Except for specific mentions, the numerical computations utilize the following fixed parameters:  $t = 10$ ,  $\alpha = 20^\circ$ ,  $K = 2$ ,  $M = 2$ ,  $Pr = 7.0$ ,  $\alpha_d = 0.5$ ,  $D_p = 10$ , and  $\gamma = 0.1$ . The parameter numerical ranges considered in the figures are  $K = 0.5, 1, 2, 3$ ,  $M = 0, 1, 2, 4$ ,  $\alpha_d = 0.5, 1, 1.5, 2$ ,  $D_p = 1, 3, 5, 10$ , and  $Pr = 0.7, 1, 3, 7$ . Table 1 illustrates the validation of the obtained results through comparison with the findings of [46, 47] on a limiting case. This comparison is conducted to validate the precision of the mathematical model proposed in the research.

The figure depicted in Figure 2 illustrates the unsteady distributions of variables  $u$  and  $u_p$  across different  $M$ . It is observed that with an increase in  $M$ , the time required to achieve a steady state increases for the fluid phase but decreases for the particle phase. This suggests differing response characteristics between the fluid and particle phases as  $M$  varies. As  $M$  increases, the magnetic forces exerted on the fluid become stronger. This results in greater resistance to fluid motion, causing a delay in reaching a steady state. Consequently, the time required for the fluid phase to reach equilibrium increases as  $M$  rises. In contrast, particles typically respond more quickly to changes in magnetic fields

due to their smaller mass and increased susceptibility to magnetic forces. As  $M$  increases, the particles experience stronger magnetic forces, which facilitate faster alignment and adjustment to the changing field.

Figure 3 reveals the unsteady distributions of  $T$  and  $T_p$  at several numerical quantities of  $M$ . The graphic illustrates that  $T$  and  $T_p$  rises as  $M$  rises. This rise in temperatures correlates with the intensification of magnetic forces exerted on the system as  $M$  increases. Consequently, enhanced heat transfer processes leading to more efficient heat exchange mechanisms within the fluid and particles. As a result, both components of the system experience higher temperatures with increasing  $M$ . Furthermore, the attainment of a steady state becomes increasingly challenging as  $M$  rises. The system’s behavior becomes more dynamic and difficult to stabilize due to the heightened influence of magnetic forces. Consequently, there is a delay in reaching a steady state, reflected in the growing values required for equilibrium as  $M$  increases.

Figure 4 illustrates the effects of  $K$  on the velocity and temperature profiles. It has been discovered that when  $K$  is raised, both velocities rise. When  $K$  rises, the porous medium resistance decreases, improving the momentum development of the flow regime and, as a result, increasing both velocities. With increasing  $K$  values, the temperature progressively fell. An increase in  $K$  provides a porous medium that is less resistant to fluid motion, which increases flow momentum and velocity. This results in the temperature rising. Figure 5 illustrates how  $M$  affects the distribution of velocity and temperature in the fluid and particle phases. It can be observed from this figure that both velocities lessen as  $M$  grows. The strong Lorentz force causes  $M$  to increase, which resists fluid motion and progressively slows down fluid velocity. Through this plot, it is clear that when  $M$  surges, the temperature rises. It is evident that a higher value of  $M$  promotes temperature dispersion. A high  $M$  value typically produces a resistive force that opposes fluid flow. The boundary layer rose as a consequence. Figure 6 represents the effects of  $Pr$  on velocity and temperature distribution, respectively. Through this plot, it can be seen that both  $U$  and  $U_p$  dropped off as  $Pr$  rose since the fluid became more viscous as  $Pr$  rose. The temperature dropped gradually for higher values of  $Pr$ . The boundary layer thickness decreases as  $Pr$  rises. A higher  $Pr$  fluid has a thermal diffusivity that is comparatively low, thus reducing conduction and the boundary layer thickness and enhancing the heat transfer rate.

Figure 7 depicts the impacts of  $\alpha_d$  on velocity and temperature distribution, respectively. It is interesting to find that the growth of  $\alpha_d$  boosts  $U_p$  while dropping  $U$ . The fluid velocity drives the movement of the particle, and also note that the particles slip along the cone so that the the fluid velocity is decreasing and the particle velocity is increasing until they achieve almost the same velocity in the fluid phase. Moreover, the same

**Table 1.** Comparison of  $Nu_x/Gr_L^{1/4}$  at  $\zeta = 1$ .

$Pr$	0.03	0.1	0.7	1.0
[46] $-\theta'(0) * \sqrt{Pr}$	0.1244	0.2113	0.4511	0.5104
[47] $Nu_x/Gr_L^{1/4}$	0.1243	0.2115	0.4529	0.5125
Present Results $Nu_x/Gr_L^{1/4}$	0.1247	0.2124	0.4591	0.5211



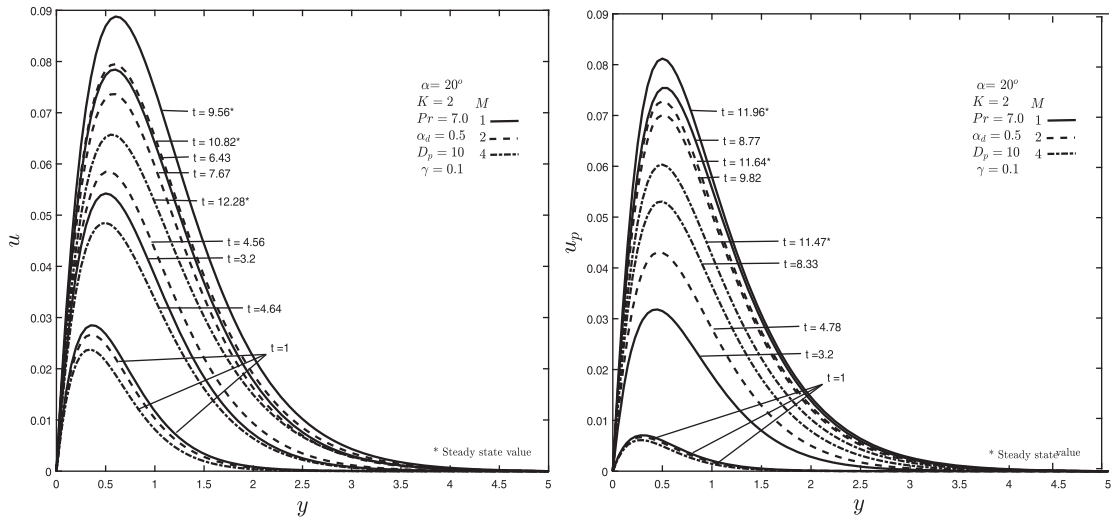


Figure 2. Variations in fluid and particle velocity under varied magnetic field.

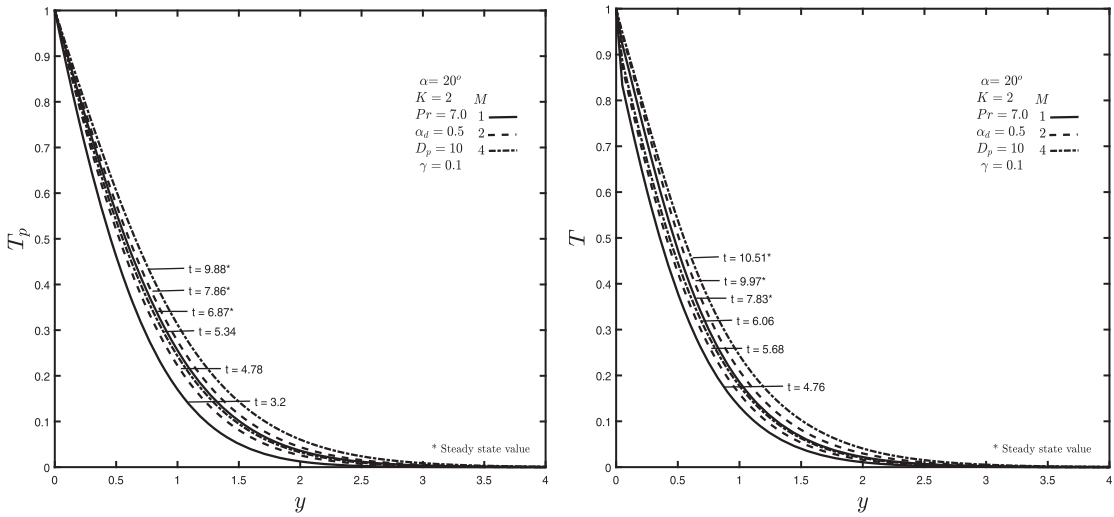


Figure 3. Variations in fluid and particle temperature under varied magnetic field.

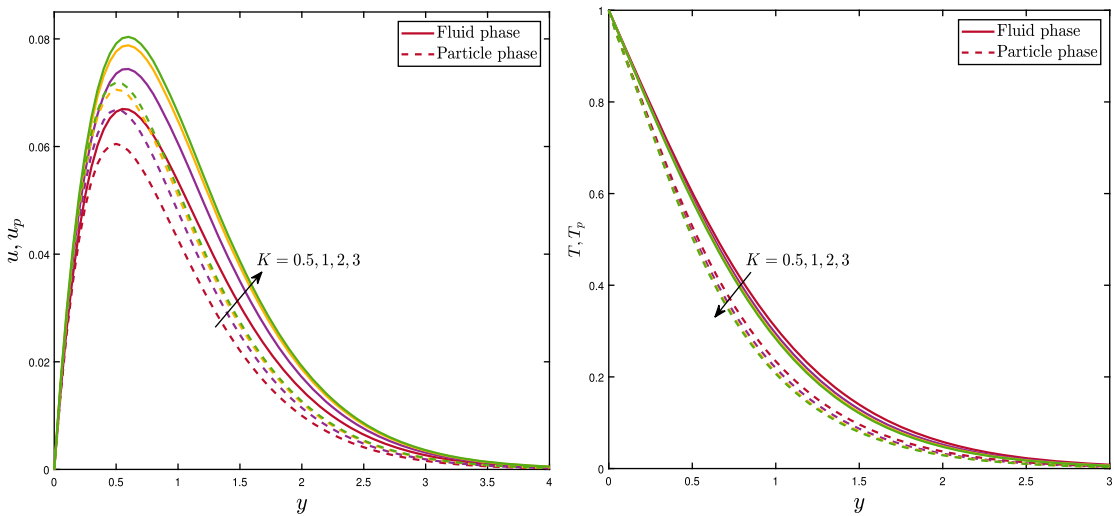


Figure 4. Variational effects of porous permeability on velocity and temperature distribution.

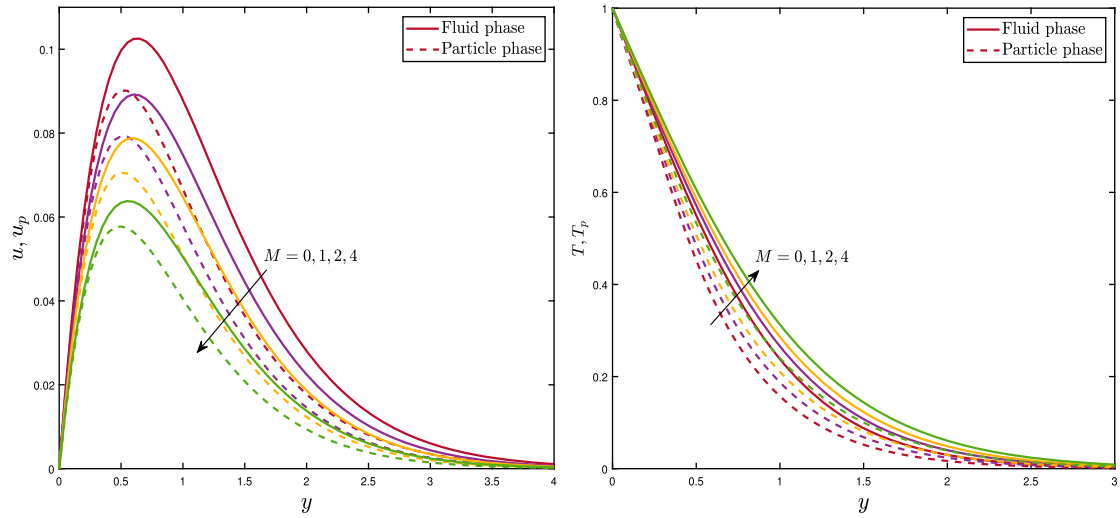


Figure 5. Variational effects of magnetic field on velocity and temperature distribution.

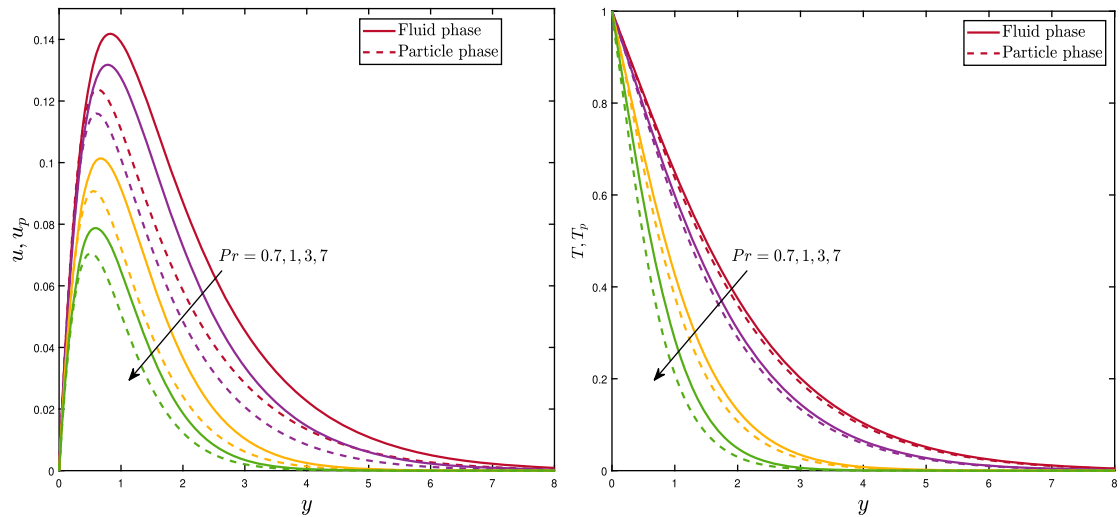


Figure 6. Variational effects of Prandtl number on velocity and temperature distribution.

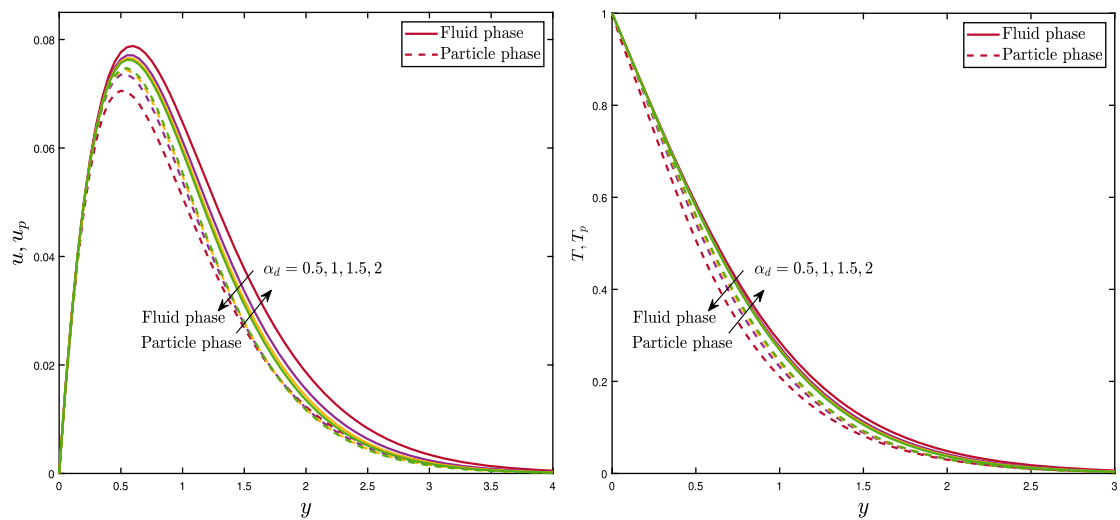
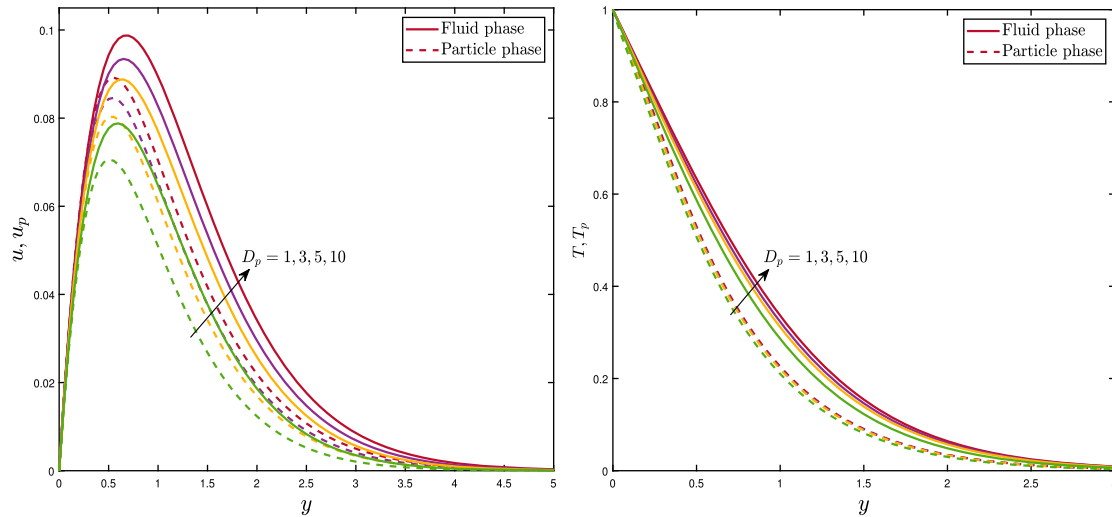


Figure 7. Variational effects of fluid-particle interaction on velocity and temperature distribution.



**Figure 8.** Variational effects of mass concentration of particle phase on velocity and temperature distribution.

**Table 2.** Influence of  $t$  on  $Nu_x/Gr_L^{1/4}$  and  $\tau_x/Gr_L^{3/4}$  when  $\alpha = 20^\circ$ ,  $K = 2$ ,  $M = 2$ ,  $Pr = 7.0$ ,  $\alpha_d = 0.5$ ,  $D_p = 10$ , and  $\gamma = 0.1$ .

$t$	1	3.2	4.65	5.23	8.78	10
$Nu_x/Gr_L^{1/4}$	2.1513	1.3711	1.1623	1.0999	0.9221	0.9078
$\tau_x/Gr_L^{3/4}$	0.1699	0.2372	0.2642	0.2730	0.3071	0.3100

**Table 3.** Influence of  $t$ ,  $K$ ,  $M$ ,  $Rd$ ,  $Q$  and  $\alpha_d$  on  $Nu_x/Gr_L^{1/4}$  and  $\tau_x/Gr_L^{3/4}$ .

$Pr$	$D_p$	$\gamma$	$K$	$M$	$\alpha_d$	$Nu_x/Gr_L^{1/4}$	$\tau_x/Gr_L^{3/4}$
0.7	10	0.1	2	2	0.5	0.3671	0.4225
1						0.4253	0.4075
3						0.6482	0.3567
7	1					0.7785	0.3486
	3					0.8097	0.3397
	5					0.8376	0.3316
	10		0.5			0.8685	0.2815
			1			0.8900	0.3011
			3			0.9085	0.3164
			2	0		0.9885	0.3715
				1		0.9383	0.3386
				4		0.8598	0.2730
				2		0.5198	0.3573
					1	0.9039	0.3110
					1.5	0.9063	0.3104
					2	0.9078	0.3100

behaviour is captured in temperature distribution.  $T_p$  is influenced by the factors of the thermal relaxation time and the relative velocity between the phases. When  $\alpha_d$  considerably large, the relative velocity between phases is reduced, and thermal relaxation time also shortens.

As shown by Figure 8, the distribution of velocity and temperature in the fluid and particle phases is affected by  $D_p$ . When  $D_p$  is raised, both velocities and temperatures are discovered to boost. The table presented in Table 2 illustrates the impact of  $t$  on  $Nu_x/Gr_L^{1/4}$  and  $\tau_x/Gr_L^{3/4}$ . The values of  $\tau_x/Gr_L^{3/4}$  increase whereas the values of  $Nu_x/Gr_L^{1/4}$  fall as  $t$  increases. Table 3 depicts the impacts of  $K$ ,  $M$ ,  $\alpha_d$ , and  $D_p$  on  $Nu_x/Gr_L^{1/4}$  and  $\tau_x/Gr_L^{3/4}$ . It is clear that  $Nu_x/Gr_L^{1/4}$  rises when the numbers of  $Pr$ ,  $D_p$ ,  $K$ , and  $\alpha_d$  boost while dropping as the number of  $M$

enhances. Furthermore,  $\tau_x/Gr_L^{3/4}$  goes down as the number of  $Pr$ ,  $M$ , and  $\alpha_d$  rises while going up with an increase of  $D_p$  and  $K$ .

#### 4. Conclusion

It has been investigated and taken into consideration to solve the problem of unsteady dusty flow with magnetic field effects over a non-isothermal vertical cone. MATLAB programming software was used to present the problem's formulation and solutions. Dusty fluid flow across vertical cone surfaces provides valuable insights that have applications in automotive and aerospace engineering. Finding areas that are vulnerable to flow separation and turbulence can be aided by examining the behaviour of dusty particles within the boundary layer. The results of this study are outlined as follows:

- The velocity profiles of both the fluid and dust phases rise with increasing porosity parameter values.
- On the contrary, elevating the magnetic parameter, fluid-particle interaction parameter, and mass concentration of the particle phase parameter results in decreased velocity profiles.
- Additionally, a higher magnetic parameter and mass concentration of the particle phase parameter correlate with elevated temperature distributions.
- Conversely, the fluid-particle interaction parameter and the porosity parameter exhibit an inverse relationship with temperature distribution.

#### Disclosure statement

No potential conflict of interest was reported by the author(s).

#### Funding

The authors would like to acknowledge the financial support from Universiti Teknologi Malaysia for the funding under UTM Fundamental Research (UTMFR: Q.J130000.3854.23H22).



## ORCID

Hajar Hanafi  <http://orcid.org/0000-0002-0065-5723>  
 Hanifa Hanif  <http://orcid.org/0000-0003-0053-0653>  
 Sharidan Shafie  <http://orcid.org/0000-0001-7795-2278>

## References

- [1] Sproull WT. Viscosity of dusty gases. *Nature*. 1961;190: 976–978. doi: [10.1038/190976a0](https://doi.org/10.1038/190976a0)
- [2] Siddiqa S, Hossain MA, Saha SC. Two-phase natural convection flow of a dusty fluid. *Int J Numer Methods Heat Fluid Flow*. 2015;25:1542–1556. doi: [10.1108/HFF-09-2014-0278](https://doi.org/10.1108/HFF-09-2014-0278)
- [3] Turkyilmazoglu M. Bödewadt flow and heat transfer of dusty fluid with Navier slip. *Arch Mech*. 2022;74(2-3):157–172.
- [4] Dey D, Makinde OD, Chutia B. Hydromagnetic flow of dusty fluid with heat and mass transfer past a stretching curved surface in a porous medium. *Lat Am Appl Res*. 2022;52:201–206.
- [5] Ramesh G, Gireesha B, Gorla RSR. Boundary layer flow past a stretching sheet with fluid-particle suspension and convective boundary condition. *Heat Mass Transf*. 2015;51:1061–1066. doi: [10.1007/s00231-014-1477-z](https://doi.org/10.1007/s00231-014-1477-z)
- [6] Jagannadham MN, Rath B, Dash D. Numerical solution of fluid and particle phase on velocity of heat with effect of magnetic field in incompressible dusty fluid. *Dogo Rangsang Research Journal*. 2022;12(10):120–127.
- [7] Reddimalla N, Ramana Murthy J, Radha Krishna Murthy, et al. Effect of Magnetic Field on Unsteady Flow of Dusty Fluid Due to Constant Pressure Gradient Through a Circular Cylinder: An Analytical Treatment. In *Recent Advances in Applied Mathematics and Applications to the Dynamics of Fluid Flows: 5th International Conference on Applications of Fluid Dynamics (ICAFD) 2020*, Singapore: Springer Nature Singapore. 2022;195–202.
- [8] Kumar S. Hydro Magnetic Mixed Convection And Mass Transfer Flow of a Viscoelastic Fluid through a Porous Medium Confined in a Vertical Channel: a Comparison between Crank-Nicolson Method and Laplace Transform Technique. *International Journal Of Multidisciplinary Research In Science, Engineering and Technology*. 2021;4(3):418–425.
- [9] Platzman RL. *Cosmical electrodynamics*. H. Alfven. New York: Oxford Univ. Press; 1950; p. 237. 5.00. Science. 1950;112:507. doi: [10.1126/science.112.2913.507.b](https://doi.org/10.1126/science.112.2913.507.b)
- [10] Hanif H, Lund LA, Shafie S. Dynamics of  $ag-ceTiO_2/H_2O$  between two coaxial cylinders: a computational approach. *Eur Phys J Plus*. 2023;138:1–10. doi: [10.1140/epjp/s13360-022-03580-z](https://doi.org/10.1140/epjp/s13360-022-03580-z)
- [11] Hanif H, Shafie S. Impact of  $Al_2O_3$  in electrically conducting mineral oil-based Maxwell nanofluid: application to the petroleum industry. *Fractal Fract*. 2022;6:180. doi: [10.3390/fractalfract6040180](https://doi.org/10.3390/fractalfract6040180)
- [12] Hanif H, Shafie S. Application of Cattaneo heat flux to Maxwell hybrid nanofluid model: a numerical approach. *Eur Phys J Plus*. 2022;137:989. doi: [10.1140/epjp/s13360-022-03209-1](https://doi.org/10.1140/epjp/s13360-022-03209-1)
- [13] Saqib M, Hanif H, Abdeljawad T, et al. Heat transfer in MHD flow of Maxwell fluid via fractional Cattaneo–Friedrich model: a finite difference approach. *Comput Mater Contin*. 2020;65:1959–1973.
- [14] Abbas W, Khaled O, Beshir S, et al. Analysis of chemical, Ion Slip, and thermal radiation effects on an Unsteady MHD Dusty fluid flow with heat and mass transfer through a Porous Media between parallel plates. 2022.
- [15] Hanif H, Khan I, Shafie S. MHD natural convection in cadmium telluride nanofluid over a vertical cone embedded in a porous medium. *Phys Scr*. 2019;94:125208. doi: [10.1088/1402-4896/ab36e1](https://doi.org/10.1088/1402-4896/ab36e1)
- [16] Hanif H, Khan I, Shafie S, et al. Heat transfer in cadmium telluride-water nanofluid over a vertical cone under the effects of magnetic field inside porous medium. *Processes*. 2019;8:7. doi: [10.3390/pr8010007](https://doi.org/10.3390/pr8010007)
- [17] Hanif H, Shafie S, Jagun ZT. Maximizing thermal efficiency of a cavity using hybrid nanofluid. *J Clean Prod*. 2024;441:141089. doi: [10.1016/j.jclepro.2024.141089](https://doi.org/10.1016/j.jclepro.2024.141089)
- [18] Reyaz R, Mohamad AQ, Lim YJ, et al. Analytical solution for impact of Caputo–Fabrizio fractional derivative on MHD casson fluid with thermal radiation and chemical reaction effects. *Fractal Fract*. 2022;6:38. doi: [10.3390/fractalfract6010038](https://doi.org/10.3390/fractalfract6010038)
- [19] Noor NAM, Admon MA, Shafie S. Unsteady MHD squeezing flow of casson fluid over horizontal channel in presence of chemical reaction. *J Adv Res Fluid Mech Therm Sci*. 2022;92:49–60. doi: [10.37934/arfmts](https://doi.org/10.37934/arfmts)
- [20] Hanif H, Shafie S, Jagun Z. Maximizing heat transfer and minimizing entropy generation in concentric cylinders with  $CuO-MgO-TiO_2$  nanoparticles. *Chin J Phys*. 2023;89:493–503.
- [21] Merk H, Prins J. Thermal convection in laminar boundary layers II. *Appl Sci Res Sect A*. 1954;4:195–206. doi: [10.1007/BF03184951](https://doi.org/10.1007/BF03184951)
- [22] Awad F, Sibanda P, Motsa SS, et al. Convection from an inverted cone in a porous medium with cross-diffusion effects. *Comput Math Appl*. 2011;61:1431–1441. doi: [10.1016/j.camwa.2011.01.015](https://doi.org/10.1016/j.camwa.2011.01.015)
- [23] Makanda G, Makinde O, Sibanda P, et al. Natural convection of viscoelastic fluid from a cone embedded in a porous medium with viscous dissipation. *Math Probl Eng*. 2013;2013:1–11. doi: [10.1155/2013/934712](https://doi.org/10.1155/2013/934712)
- [24] Jasmine Benazir A, Sivaraj R, Makinde OD. Unsteady magnetohydrodynamic casson fluid flow over a vertical cone and flat plate with non-uniform heat source/sink. *Int J Eng Res Afr*. 2016;21:69–83. doi: [10.4028/www.scientific.net/JERA.21](https://doi.org/10.4028/www.scientific.net/JERA.21)
- [25] Hanif H, Khan A, Rijal Illias M, et al. Significance of  $Cu-Fe_3O_4$  on fractional Maxwell fluid flow over a cone with Newtonian heating. *J Taibah Univ Sci*. 2024;18:2285491. doi: [10.1080/16583655.2023.2285491](https://doi.org/10.1080/16583655.2023.2285491)
- [26] Basha HT, Gunakala SR, Makinde OD, et al. Chemically reacting unsteady flow of nanofluid over a cone and plate with activation energy. *Defect and Diffusion Forum*. 2018;387:343–351. Switzerland: Trans Tech Publications Ltd.
- [27] Turkyilmazoglu M. On the fluid flow and heat transfer between a cone and a disk both stationary or rotating. *Math Comput Simul*. 2020;177:329–340. doi: [10.1016/j.matcom.2020.04.004](https://doi.org/10.1016/j.matcom.2020.04.004)
- [28] Ilyas A, Ashraf M, Rashad A. Periodical analysis of convective heat transfer along electrical conducting cone embedded in porous medium. *Arab J Sci Eng*. 2022;47:8177–8188. doi: [10.1007/s13369-021-06191-5](https://doi.org/10.1007/s13369-021-06191-5)
- [29] Siddiqa S, Begum N, Hossain M, et al. Two-phase dusty fluid flow along a cone with variable properties. *Heat Mass Transf*. 2017;53:1517–1525. doi: [10.1007/s00231-016-1918-y](https://doi.org/10.1007/s00231-016-1918-y)
- [30] Siddiqa S, Begum N, Hossain AM, et al. Numerical solution of contaminated oil along a vertical wavy frustum of a cone. *Therm Sci*. 2018;22:2933–2942. doi: [10.2298/TSCI160425231S](https://doi.org/10.2298/TSCI160425231S)
- [31] Mahanthesh B, Makinde OD, Gireesha BJ, et al. Two-phase flow of dusty Casson fluid with Cattaneo-Christov

- heat flux and heat source past a cone, wedge and plate. Defect and Diffusion Forum. 2018;387:625–639. Switzerland: Trans Tech Publications Ltd.
- [32] Palani G, Kumar EL. Dusty gas flow over a semi-infinite vertical cone. JP Journal of Heat and Mass Transfer. 2021;22(2):201–216. India: Pushpa Publishing House.
- [33] Turkyilmazoglu M. A note on the induced flow and heat transfer due to a deforming cone rotating in a quiescent fluid. J Heat Transf. 2018;140:124502. doi: [10.1115/1.4041184](https://doi.org/10.1115/1.4041184)
- [34] Turkyilmazoglu M. The flow and heat in the conical region of a rotating cone and an expanding disk. Int J Numer Methods Heat Fluid Flow. 2023;33:2181–2197. doi: [10.1108/HFF-11-2022-0655](https://doi.org/10.1108/HFF-11-2022-0655)
- [35] Berlemont A, Desjonqueres P, Gouesbet G. Particle lagrangian simulation in turbulent flows. Int J Multiph Flow. 1990;16:19–34. doi: [10.1016/0301-9322\(90\)90034-G](https://doi.org/10.1016/0301-9322(90)90034-G)
- [36] Saffman P. On the stability of laminar flow of a dusty gas. J Fluid Mech. 1962;13:120–128. doi: [10.1017/S0022112062000555](https://doi.org/10.1017/S0022112062000555)
- [37] Hanif H. Cattaneo–Friedrich and Crank–Nicolson analysis of upper-convected Maxwell fluid along a vertical plate. Chaos Solitons Fract. 2021;153:111463. doi: [10.1016/j.chaos.2021.111463](https://doi.org/10.1016/j.chaos.2021.111463)
- [38] Hanif H. A finite difference method to analyze heat and mass transfer in kerosene based  $\gamma$ -oxide nanofluid for cooling applications. Phys Scr. 2021;96:095215. doi: [10.1088/1402-4896/ac098a](https://doi.org/10.1088/1402-4896/ac098a)
- [39] Hanif H. A computational approach for boundary layer flow and heat transfer of fractional Maxwell fluid. Math Comput Simul. 2022;191:1–13. doi: [10.1016/j.matcom.2021.07.024](https://doi.org/10.1016/j.matcom.2021.07.024)
- [40] Blottner F. Finite difference methods of solution of the boundary-layer equations. AIAA J. 1970;8:193–205. doi: [10.2514/3.5642](https://doi.org/10.2514/3.5642)
- [41] Hanafi H, Hanif H, Shafie S, et al. Unsteady free convection dusty MHD flow with dissipation effect over non-isothermal vertical cone. J Adv Res Fluid Mech Therm Sci. 2024;114:56–68. doi: [10.37934/arfmst](https://doi.org/10.37934/arfmst)
- [42] Sivaraj R, Kumar BR. Viscoelastic fluid flow over a moving vertical cone and flat plate with variable electric conductivity. Int J Heat Mass Transf. 2013;61:119–128. doi: [10.1016/j.ijheatmasstransfer.2013.01.060](https://doi.org/10.1016/j.ijheatmasstransfer.2013.01.060)
- [43] Pullepu B, Ekambavanan K, Chamkha A. Unsteady laminar natural convection from a non-isothermal vertical cone. Nonlinear Anal Model Control. 2007;12:525–540. doi: [10.15388/NA.2007.12.4.14684](https://doi.org/10.15388/NA.2007.12.4.14684)
- [44] Pullepu B, Chamkha AJ, Pop I. Unsteady laminar free convection flow past a non-isothermal vertical cone in the presence of a magnetic field. Chem Eng Commun. 2012;199:354–367. doi: [10.1080/00986445.2011.592443](https://doi.org/10.1080/00986445.2011.592443)
- [45] Thandapani E, Ragavan A, Palani G. Finite-difference solution of unsteady natural convection flow past a non-isothermal vertical cone under the influence of a magnetic field and thermal radiation. J Appl Mech Tech Phys. 2012;53:408–421. doi: [10.1134/S0021894412030133](https://doi.org/10.1134/S0021894412030133)
- [46] Hering R, Grosh R. Laminar free convection from a non-isothermal cone. Int J Heat Mass Transf. 1962;5:1059–1068. doi: [10.1016/0017-9310\(62\)90059-5](https://doi.org/10.1016/0017-9310(62)90059-5)
- [47] Sambath P. A Study on Unsteady Natural Convective Flow past a Vertical Cone with Heat and Mass Transfer Effects. 2017.